Quantitative Estimation of Strong Winds in an Urban District during Typhoon Jebi (2018) by Merging Mesoscale Meteorological and Large-Eddy Simulations

Tetsuya Takemi, Toshiya Yoshida, Shota Yamasaki, and Kentaro Hase
Disaster Prevention Research Institute, Kyoto University, Uji, Japan

Abstract

An intense tropical cyclone, Typhoon Jebi (2018), landed the central part of Japan and caused severe damages. Quantitative assessment of strong winds in urban districts under typhoon conditions is important to understand the underlying risks. As a preliminary study, we investigate the influences of densely built urban environments on the occurrence of wind gusts in an urban district of Osaka City during Typhoon Jebi by merging mesoscale meteorological and building-resolving large-eddy simulations (LES). With the successful reproduction of the track and intensity of the typhoon in meteorological simulations, the simulated winds at the boundary-layer top of the LES model are used to quantitatively estimate the wind gusts in the urban district. The maximum wind gust in the analysis area of Osaka was estimated as 60−70 m s^{-1}, which is comparable to the wind speed at the height of about 300 m.

(**Citation**: Takemi, T., T. Yoshida, S. Yamasaki, and K. Hase, 2018: Quantitative estimation of strong winds in an urban district during Typhoon Jebi (2018) by merging mesoscale meteorological and large-eddy simulations. *SOLA*, **15**, 22−27, doi:10.2151/sola.2019-005.)

1. Introduction

Typhoons are one of the major extreme weather in the western North Pacific region, and sometimes become a great threat to our society. Recently Typhoon Haiyan (2013) made landfall over the Philippines and caused devastating damages by storm surges (Mori et al. 2014). Historically, Japan faced severe damages due to strong winds by intense typhoons such as Vera (1959), Nancy (1961), Mireille (1991), and Songda (2004). Most recently, Typhoon Jebi (2018) made landfall on the islands of Shikoku and Honshu, crossing over the Osaka Bay, and spawned storm surges/high waves around the bay areas as well as strong winds over the inland areas. Kansai International Airport (KIX) established on a reclaimed island in the Osaka Bay in 1994 was seriously damaged by storm surge. Furthermore, a large number of points observed extreme winds, which caused severe damages to houses/buildings, trees/forests, power lines, etc. (Cabinet Office 2018).

Typhoon Jebi obtained the lifetime minimum central pressure of 915 hPa (according to Regional Specialized Meteorological Center Tokyo) and took a track very similar to Typhoon Nancy (1961) (i.e., Daini-Muroto Typhoon) and Muroto Typhoon in 1934. In Osaka City, the 1st, 2nd, and 3rd highest record of instantaneous wind speed is 60.0 m s^{-1} in September 1934 (Muroto), 50.6 m s^{-1} in September 1961 (Daini-Muroto), and 47.4 m s^{-1} in September 2018 (Jebi), respectively, suggesting that a typhoon has been the most threatening windstorm in the area. Considering the time period spanning from 1934 to 2018, the influences of urbanization and global warming should be taken into account to assess the disaster risks by typhoons. This study focuses on the influences of urban buildings and structures on the development of strong winds by Typhoon Jebi.

Buildings and structures in urban areas affect most significantly the magnitude of wind gustiness. Kato et al. (1992) demonstrated that gust factors during typhoons exceed 2 within the urban canopy from measurements in Tokyo and Yokohama. By combining mesoscale meteorological and large eddy simulation (LES) models, Nakayama et al. (2012) successfully estimated the instantaneous wind speeds with gust factors exceeding 2 in a business district of Tokyo during a typhoon landfall. As indicated in Yoshida et al. (2018) and Yoshida and Takemi (2018), the variability of wind speed become more significant with a larger variability of building height. These studies suggest that densely built urban districts would be susceptible to typhoon-induced stronger winds than previously thought from the past experiences such as Muroto and Daini-Muroto Typhoons. Thus, quantitatively estimating the strong winds in real urban districts by Typhoon Jebi (2018) is a scientific challenge and is very important for assessing risks of strong winds in urban districts.

As a preliminary study, we estimate quantitatively the strong winds within a business district of Osaka City during Typhoon Jebi (2018) by employing a mesoscale meteorological and an LES model. By explicitly representing real buildings and structures in LES, this study examines complex/complicated characteristics of winds within the densely built urban environment.

2. Procedure of numerical analysis

This study used both a mesoscale meteorological model and a building-resolving LES model. The meteorological model was intended to simulate the typhoon and its meteorological background, while the LES model simulated turbulent airflows within a business district of Osaka.

2.1 Meteorological model settings

The meteorological model used was the Weather Research and Forecasting (WRF) model/the Advanced Research WRF (Skamarock et al. 2008) version 4.0. We set two-way-nested computational domains (Fig. 1a): Domain 1 covers parts of the western North Pacific and the Japanese islands at the 4.5-km horizontal grid, and Domain 2 covers mainly the Kinki region at the 0.9-km grid on the Lambert conformal projection. The both domains have 56 vertical levels, with the interval extended with height up to the top at the 20-hPa level. The model topography was created from the 30-arc-seconds elevation data from the United States Geological Survey, while the land-use characteristics were determined by the MODIS-based 21-category data.

We set the physics parameterizations similar to those employed in Takemi et al. (2016a, 2016b) and Nayak and Takemi (2019): e.g, the 6-category single-moment microphysics scheme of Hong and Lim (2006); the Yonsei University boundary-layer scheme (Hong et al. 2006), and a Monin-Obukhov similarity-based surface-flux scheme (Jiménez et al. 2012). No cumulus parameterization was used.

The 6-hourly Global Spectral Model analyses of Japan Meteorological Agency were used to prescribe the initial and boundary conditions for the atmospheric and surface states. Merged satellite and in situ data Global Daily Sea Surface Temperatures

Corresponding author: Tetsuya Takemi, Disaster Prevention Research Institute, Kyoto University, Gokasho, Uji, Kyoto 611-0011, Japan. E-mail: takemi@storm.dpri.kyoto-u.ac.jp.

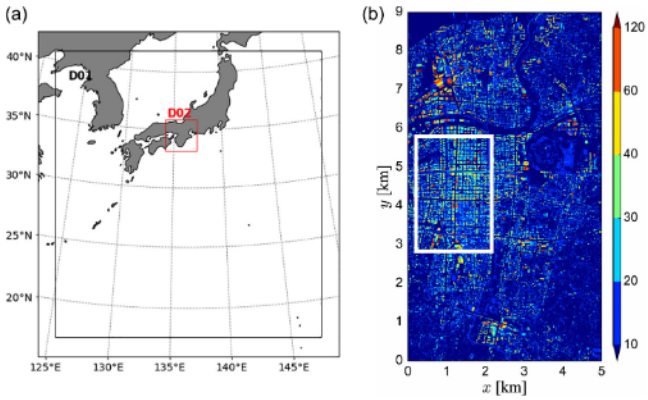

Fig. 1. The computational domains for (a) the WRF model and (b) the LES model. In (a), two nested domains (D01: Domain 1; D02: Domain 2) were exhibited. In (b), the main computational domain is indicated by white solid box, having a 3 km (south-north) by 2 km (west-east) area within Osaka City. The color denotes the height of the buildings and structures obtained from the 2-m-mesh DSM data.

(MGDSST) data were used for prescribing SSTs. To accelerate the development of the typhoon from the analyses, we added an initial vortex from a typhoon-bogus scheme. With the initial times changed from 1200 UTC 31 August to 1200 UTC 2 September 2018 at the 6-hour interval, time integration was done until 1800 UTC 4 September and totally conducted 9 simulations. The simulated outputs for Domain 2 were done at 10-minute interval and used for the following analysis.

2.2 Building-resolving LES modeling

We used the LES model developed by Yoshida et al. (2018), based on Nakayama et al. (2011). The governing equations consist of the filtered incompressible continuity and Navier-Stokes equations with the subgrid-scale eddy viscosity parameterized by the standard Smagorinsky model (Smagorinsky 1963; Pope 2000). The equations were discretized on the Cartesian coordinate. Buildings were immersed in this coordinate and were represented as an external forcing to the Navier-Stokes equation (Goldstein et al. 1993). The LES model was well validated against the observations in an urban area of Kyoto City (Yoshida et al. 2018), and thus is applicable to this study.

The buildings in Osaka were represented in LES with the use of 2-m-mesh digital surface model (DSM) data of Kokusai Kogyo Co., Ltd. With this dataset, buildings were explicitly placed on the lower boundary of the main computational domain having a 3 km (south-north) by 2 km (west-east) area (Fig. 1b) with the depth of 1.026 km with buffer regions surrounding the main domain. The horizontal grid spacing was 2 m, while the vertical grid spacing was 2 m from the bottom to the 350-m height and was stretched from 2 m to 16 m above the 350-m height until the model top. Note that the horizontal grid spacing was the same as the DSM resolution, and hence the simulation here employed the highest resolution that was able to be set with the current DSM dataset.

Since the dominant wind direction during the typhoon passage was generally south, the streamwise direction of the LES domain was set from south to north. This means that the inflow (outflow) boundary of the main computational domain was set at the southern (northern) boundary. At this inflow boundary, turbulent flows generated in a driver domain were imposed in the same way as in Yoshida et al. (2018) and Yoshida and Takemi (2018) (See Supplement 1). At the outflow boundary a radiation condition was prescribed, while at the lateral (i.e., western/eastern) boundaries the periodic condition was imposed.

From the WRF simulations, we found that the vertical motion in the analysis area is significantly weaker than the horizontal motion, the stability below the level of about 300−400 m is near-neutral, and westerly winds are weaker than southerly winds (not shown). Thus, the assumption of no mean vertical motion, neutral condition, and southerly inflow in LES is validated.

The time integration was conducted for 5400 seconds; the outputs during the last 1800 seconds were used for the analysis. The wind speeds were normalized by the reference wind speed U_∞ defined as the wind at the boundary-layer top, i.e., the 326-m height (z_∞) which was chosen as the height at which the maximum of the mean horizontal winds appeared (see Fig. 5). Note here that this boundary-layer height is different from the actual one under the typhoon condition. The idea for this normalization was to use the WRF outputs as a reference to obtain quantitative values for wind speeds within urban canopy, as described in Section 3.2. Ahmad et al. (2017) demonstrated the usefulness of this normalization to assess gust intensities within urban canopies at different locations.

2.3 Merging meteorological and LES models

There are some approaches in merging meteorological and LES models (e.g. Mayor et al. 2002; Mochida et al. 2011; Nakayama et al. 2012; Muñoz-Esparza et al. 2014; Li et a. 2017; Huang et al. 2018): the outputs of a meteorological model are somehow directly imposed as the inflow conditions of an LES model. In this preliminary study, we employed a simple approach to use winds only at a certain height from the meteorological model as a reference for airflows simulated in LES (Takemi et al. 2006). The idea for this analysis is to combine the advantages of the both WRF and LES models: the WRF simulation provides the meteorologically driven wind speeds U_{WRF} at z_∞, while the LES defines the ratio of wind speed U_z within urban canopy layer against U_∞.

Thus, wind speed at height z within the urban canopy is determined as follows:

$$U(z) = \frac{U_z}{U_\infty} U_{WRF}. \quad (1)$$

Normalized wind speed from LES is dimensionalized with the aid of the WRF results.

3. Results

To quantitatively estimate strong winds within a specific area, we need to closely reproduce the track and intensity of a typhoon in meteorological simulations (Takemi et al. 2016c). Figure 2 shows the tracks of the simulated typhoons as well as the best track. Overall the simulations well capture the best track (Fig. 2a), while a closer look at the results indicates some departures from the best track (Fig. 2b). The case initialized at 1800 UTC 1 September performs the best especially over the Osaka Bay.

The intensity of the simulated typhoons is examined in Fig. 3. The use of the typhoon bogus facilitates the typhoon development and thus the typhoon intensity especially after 0600 UTC 3 September is favorably reproduced. Specifically, the central pressure after 1800 UTC 3 September is closely captured in the cases initialized at 1200 UTC 1 September and later. In these cases the maximum wind speed is also reproduced, although earlier weakening of the maximum wind than in the best track is noted. This weakening is due to sharper decrease of winds by surface roughness than would actually occur, after landfall over the Shikoku and Awaji islands. In spite of this discrepancy, the intensity change of the typhoon during its approach and landfall seems to be well reproduced. These results indicate that WRF performs very well in producing the track and intensity of Typhoon Jebi (2018), which renders credibility to quantitative estimations of strong winds in an urban district.

The WRF performance is further evaluated with surface wind. Figure 4 shows the times series of wind speeds at the Japan Meteorological Agency's Osaka (135.518°E, 34.682°N) and KIX (135.232°E, 34.433°N) sites. At KIX, the maximum instantaneous wind of 58.1 m s^{-1}, the highest record since the establishment, was observed. The simulated surface wind speeds, especially in the case initialized at 0000 UTC 2 September, agree with mean wind speeds in the observation at the both stations. Generally, instan-

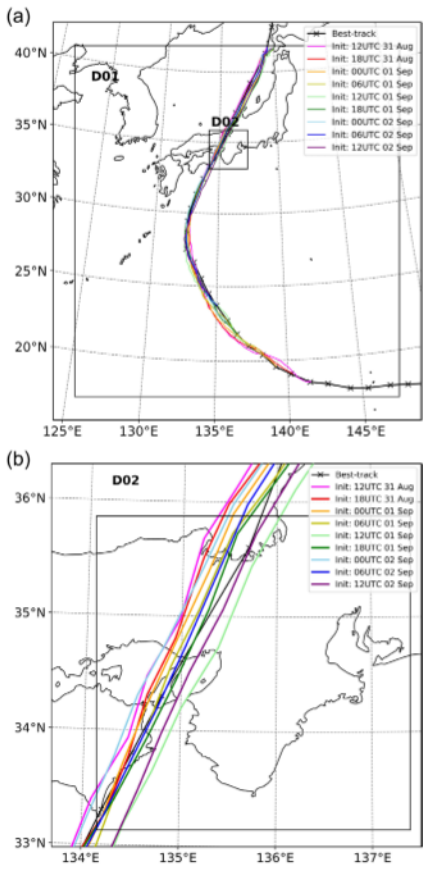

Fig. 2. The tracks of the simulated typhoons initialized at different times (ranging from 1200 UTC 31 August to 1200 UTC 2 September 2018) and the best track of Japan Meteorological Agency, shown (a) in Domain 1 and (b) in a more focused area including Domain 2.

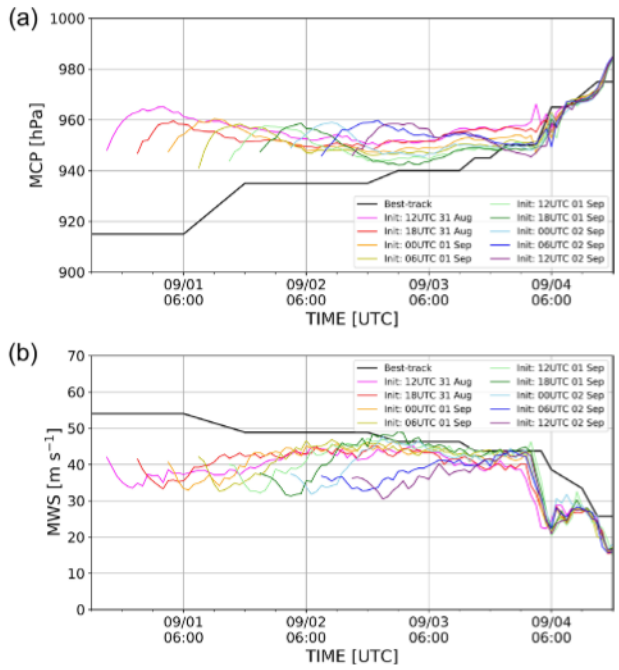

Fig. 3. The time series of the typhoon intensity in terms of (a) the central minimum pressure and (b) the maximum wind speed. Color lines denote the simulated results initialized at the different times, while the black line denotes the best track. Note that the results before the first 3 hours (i.e., spin-up period from the typhoon bogus) are not indicated.

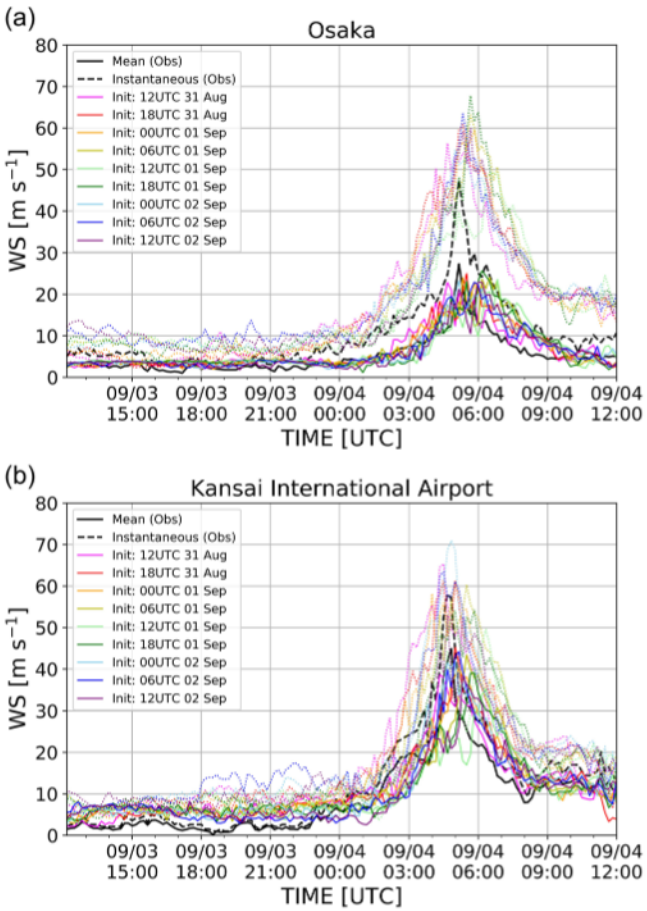

Fig. 4. The time series of the surface wind speed simulated at different times (colored solid lines) as well as the observed mean (black solid lines) and instantaneous (black dotted lines) wind speed at (a) Osaka and (b) the Kansai International Airport island (KIX). For the simulations, the wind speeds at the height z_∞ are also indicated by colored dotted lines.

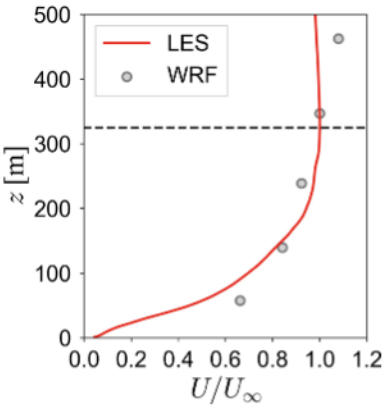

Fig. 5. The vertical profile of horizontal wind speeds simulated by WRF (denoted by gray circles) and LES (denoted by red line). The wind speeds are normalized by the wind speed at the 326-m height (z_0). The horizontal dashed line indicates the height of 326 m. For WRF, shown here is the wind speed at the point corresponding to the Osaka observation site (138.518°E, 34.682°N) at 0510 UTC 4 September 2018 when the maximum wind speed at this point was simulated. For LES, the mean winds averaged in time and space are indicated.

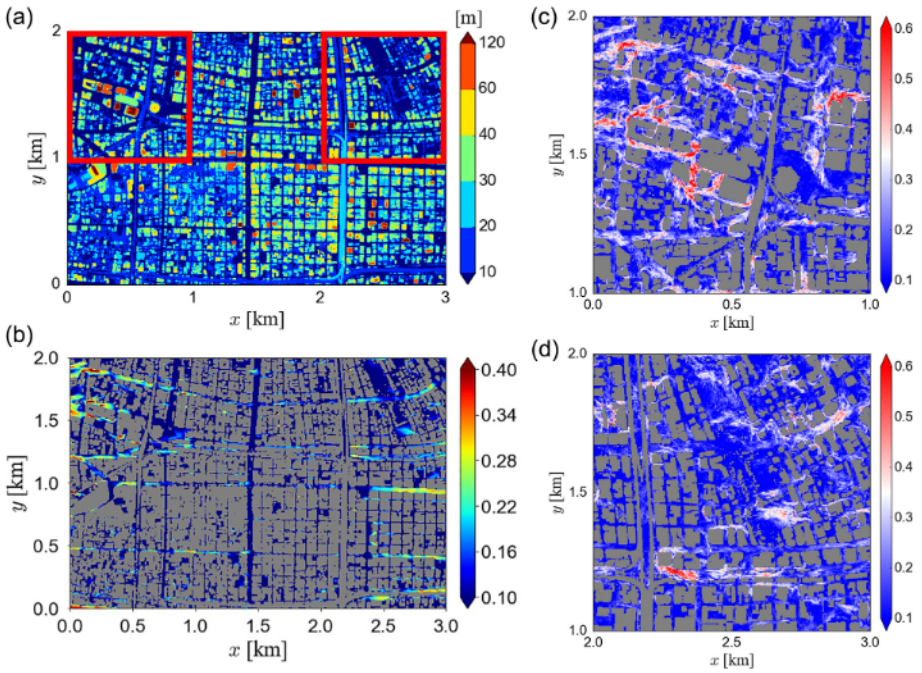

Fig. 6. (a) The computational area of 3 km by 2 km in LESs (as denoted by the white box in Fig. 1b). The left (right) side of this area is southward (northward). Color shows the height of the buildings and structures. (b) The spatial distribution of the mean wind speed at the 10-m height averaged during the simulated time period for the whole computational area. (c) (d) Instantaneous wind fields at the height of 10 m above the ground surface in the 1 km by 1 km areas denoted by (c) the red box on the left in (a) and (d) the red box on the right in (a). All the wind speeds are normalized by U_∞.

taneous winds were not reproduced well as the surface winds in WRF.

Figure 5 compares the vertical profile of wind between WRF and LES. LES reproduces sharp decrease in wind speed with the decrease in height, while WRF cannot capture this sharp decrease; this is due to the simple surface represented as roughness-length in WRF. LES has an advantage in representing the vertical profile of wind speed especially in the urban canopy layer.

The mean surface winds within the computational area of LES (Fig. 6a) are indicated in Fig. 6b. Practically, the vertical profile of mean winds over rough surfaces can be well represented by a power law. According to Architectural Institute of Japan (2015), the exponent for the power law for the rough surface with densely built, high-rise buildings is determined as 0.35. Given z_∞ as the reference height in the power law, the ratio of the wind speed at the 10-m height U_{10} to U_∞ is 0.30. Thus, the wind speed shown in Fig. 6b is overall much lower than this ratio; this is because the large variability of building height (normalized building-height variability of 0.74 in the area shown in Fig. 6a) significantly weakens the wind speed (Nakayama et al. 2011). There are some locations that have ratios comparable to 0.30 or larger around high-rise buildings and along north-south-oriented wide streets. Figures 6c and 6d exhibit the instantaneous wind fields at a certain time in the areas in Fig. 6a. In the both areas, higher winds are seen around high-rise buildings and along north-south-oriented major streets. On the other hand, wind speeds are generally lower in areas with densely built, lower-rise buildings. Such features can be found in Supplement 2, and are consistent with the airflows over the urban area of Kyoto City (Yoshida et al. 2018).

Figure 7 demonstrates the spatial distributions of the pointwise maximum U_{10} during the simulated time period. In contrast to the feature shown in Fig. 6b, Figure 7a indicates remarkable characteristics: stronger winds around the high-rise buildings and along the wide streets specifically oriented in the north-south direction, and over wide open spaces, while weaker winds within densely built areas and along some streets oriented in the east-west direction. The ratios of U_{10} to U_∞ exceed 0.8 and approach 1.0 in most locations of the strong-wind regions. Closer exhibits in the two

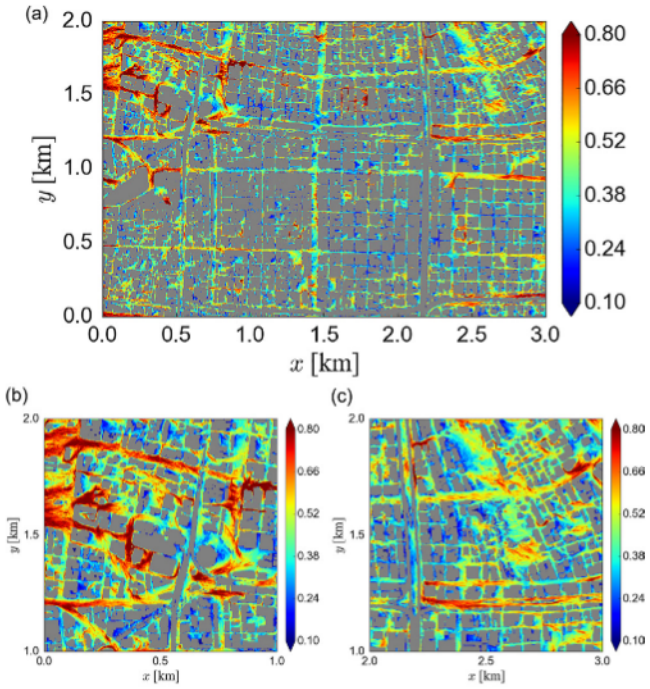

Fig. 7. The spatial distribution of the maximum instantaneous wind speed at the 10-m height from the time series of the wind speed at each grid point for (a) the whole computational area, (b) the area denoted by the red box in the left of Fig. 6a, and (c) the area denoted by the red box in the right of Fig. 6b. All the wind speed are normalized by U_∞.

areas as shown in Fig. 6a emphasize the locational characteristics of the strong-wind regions (Figs. 7b and 7c).

Based on the distributions indicated in Fig. 7, wind gusts at the surface level within the urban district are estimated with Equation (1). We can assume that the WRF winds U_{WRF} at the point corresponds to the Osaka observation site are the reference for wind U_∞ at the height of the boundary-layer top z_∞, because the spatial representativeness of winds at that height is considered to be high. From Fig. 4a, the maximum wind speeds of U_{WRF} at z_∞ simulated with the different initial times range around 60−70 m s^{-1}. When the normalized surface wind in Fig. 7 is 0.8, the surface gust becomes 48−56 m s^{-1}. With the normalized surface wind being 1.0, the surface gust becomes the same as U_{WRF}. Actually, the observed maximum gust of 47.4 m s^{-1} at the Osaka site, located in an open space in Osaka City, was within the range of the maximum gusts indicated in Fig. 7. Therefore, the maximum wind gusts within the Osaka's urban district are estimated as 50's and 60's m s^{-1}.

The areas of strong winds along the main streets correspond well with the locations of roadside trees that were severely damaged. According to Osaka City (2018), windthrows of about 1650 trees along the streets occurred. In addition, there are numerous damages to the trunks and branches of roadside trees (such as those shown in Supplement 3).

The maximum instantaneous wind speed observed at KIX seems to correspond well with the wind speed at z_∞ simulated in WRF (Fig. 4b). The enhancement of wind gusts at the surface level is considered to be due to the downward transport of high momentum at higher levels. Such downward momentum transport is seen in urban areas having buildings with variable height (Nakayama et al. 2011; Yoshida et al. 2018) and contributes to higher normalized wind speed in terms of the maxima (Fig. 7a) than in terms of the mean (Fig. 6b).

It should be mentioned here that the present resolution of 2 m is sufficient to quantitatively represent instantaneous wind speeds, considering that Nakayama et al. (2012) successfully simulated the maximum instantaneous winds in downtown Tokyo even with the 20-m resolution. Further analyses may be required to evaluate the performance of the quantitative wind simulations depending on the resolution of urban districts.

4. Conclusions

This study provides preliminary estimates of wind gusts in an urban district of Osaka City during the passage of Typhoon Jebi (2018) by merging the simulated results of the WRF model and the LES model. WRF successfully reproduced the track and intensity of the typhoon, which was able to provide the quantitative winds as a reference for the LES model. By explicitly resolving the buildings in a business district of Osaka City, LES reproduced airflows within the urban canopy and stronger winds around high-rise buildings and along major streets. The WRF winds were then used as the reference for the LES winds, which enabled to quantitatively estimate the wind gusts at the surface level in the urban district. The maximum wind gust in the analysis area was estimated as 60−70 m s^{-1}, which is comparable to the wind speed at the height of about 300 m.

This study employed the WRF/LES hybrid to estimate the wind gusts in an urban district. The limitation of this analysis is that we only used the WRF outputs at a certain height as a reference for the airflows within an urban district in the LES models. In contrast, by directly coupling the WRF and LES models through generating turbulent inflows with the WRF winds regarded as mean winds, Nakayama et al. (2012) simulated the maximum wind gust observed in Tokyo during a typhoon passage. Such direct coupling between a meteorological model and an LES (e.g., Muñoz-Esparza et al. 2014; Li et a. 2017; Huang et al. 2018) will be useful to conduct more in-depth analyses of wind gusts during strong wind events such as typhoons.

Acknowledgements

The comments by anonymous reviewers are greatly acknowledged to improve the original manuscript. This study was supported by JSPS Kakenhi 18H01680, 18K19953, and the MEXT TOUGOU program.

Edited by: R. Misumi

Supplements

Supplement 1: The setup of the driver domain.

Supplement 2: The animation showing the temporal change of the simulated surface wind speeds (U_{10}) normalized by the wind at the boundary-layer top (z_0), at the 1-second interval for a 15-minute period, in the area as denoted by the red box in the left of Fig. 6a.

Supplement 3: The pictures showing the tree damages in Osaka City.

References

Ahmad, N. H., A. Inagaki, M. Kanda, N. Onodera, and T. Aoki, 2017: Large-eddy simulation of the gust index in an urban area using lattice Boltzmann method. *Bound.-Layer Meteor.*, **163**, 447−467.

Architectural Institute of Japan, 2015: *Recommendations for Loads on Buildings*. Architectural Institute of Japan, 657 pp. (in Japanese)

Cabinet Office, 2018: A report on damages by Typhoon Jebi (2018). The version of 2 October 2018. (Available online at: http://www.bousai.go.jp/updates/h30typhoon21/pdf/301003_typhoon21_01.pdf, accessed 20 November 2018)

Goldstein, D., R. Handler, and L. Sirovich, 1993: Modeling a noslip flow boundary with an external force field. *J. Comput. Phys.*, **105**, 354−366.

Hong, S.-Y., and J. O. J. Lim, 2006: The WRF Single-Moment 6-Class Microphysics Scheme (WSM6). *J. Korean Meteor. Soc.*, **42**, 129−151.

Hong, S.-Y., Y. Noh, and J. Dudhia, 2006: A new vertical diffusion package with an explicit treatment of entrainment processes. *Mon. Wea. Rev.*, **134**, 2318−2341.

Huang, M., Y. Wang, W. Lou, and S. Cao, 2018: Multi-scale simulation of time-varying wind fields for Hangzhou Jiubao Bridge during Typhoon Chan-hom. *J. Wind Eng. Ind. Aerodyn.*, **179**, 419−437.

Jiménez, P. A., J. Dudhia, J. F. González-Rouco, J. Navarro, J. P. Montávez, and E. García-Bustamante, 2012: A revised scheme for the WRF surface layer formulation. *Mon. Wea. Rev.*, **140**, 898−918.

Kato, N., T. Ohkuma, J. R. Kim, H. Marukawa, and Y. Niihori, 1992: Full scale measurements of wind velocity in two urban areas using an ultrasonic anemometer. *J. Wind Eng. Ind. Aerodyn.*, **41**, 67−78.

Li, H., G. Cui, and Z. Zhang, 2017: A new scheme for the simulation of microscale flow and dispersion in urban areas by coupling large-eddy simulation with mesoscale models. *Bound.-Layer Meteor.*, **167**, 145−170.

Mayor, S. D., P. R. Spalart, and G. J. Tripoli, 2002: Application of a perturbation recycling method in the large-eddy simulation of a mesoscale convective internal boundary layer. *J. Atmos. Sci.*, **59**, 2385−2395.

Mochida, A., S. Iizuda, Y. Tominaga, and I. Y.-F. Lun, 2011: Upscaling CWE models to include mesoscale meteorological influences. *J. Wind Eng. Ind. Aerodyn.*, **99**, 187−198.

Mori, N., M. Kato, S. Kim, H. Mase, Y. Shibutani, T. Takemi, K. Tsuboki, and T. Yasuda, 2014: Local amplification of storm surge by Super Typhoon Haiyan in Leyte Gulf. *Geophys. Res. Lett.*, **41**, 5106−5113, doi:10.1002/2014GL060689.

Muñoz-Esparza, D., B. Kosović, J. Mirocha, and J. Beeck, 2014: Bridging the transition from mesoscale to microscale turbulence in numerical weather prediction models. *Bound.-Layer Meteor.*, **153**, 409−440.

Nakayama, H., T. Takemi, and H. Nagai, 2011: LES analysis of the aerodynamic surface properties for turbulent flows over building arrays with various geometries. *J. Appl. Meteor. Climatol.*, **50**, 1692−1712, doi:10.1175/2011JAMC2567.1.

Nakayama, H., T. Takemi, and H. Nagai, 2012: Large-eddy simulation of urban boundary-layer flows by generating turbulent inflows from mesoscale meteorological simulations. *Atmos. Sci. Lett.*, **13**, 180−186, doi:10.1002/asl.377.

Nayak, S., and T. Takemi, 2019: Dynamical downscaling of Typhoon Lionrock (2016) for assessing the resulting hazards under global warming. *J. Meteor. Soc. Japan*, **97**, in press, doi:10.2151/jmsj.2019-003.

Osaka City, 2018: A report on damages by Typhoon Jebi (2018) to roads and parks administrated by Public Works Bureau, Osaka City. (Available online at: http://www.city.osaka.lg.jp/hodoshiryo/kensetsu/0000447981.html, accessed 20 November 2018)

Pope, S. B., 2000: *Turbulent Flows*. Cambridge University Press, 771 pp.

Skamarock, W. C., J. B. Klemp, J. Dudhia, D. O. Gill, D. M. Barker, M. G. Duda, X.-Y. Huang, W. Wang, and J. G. Powers, 2008: A description of the Advanced Research WRF version 3. NCAR Tech. Note, NCAR/TN-475+STR, 113 pp.

Smagorinsky, J., 1963: General circulation experiments with the primitive equations. *Mon. Wea. Rev.*, **91**, 99−164.

Takemi, T., T. Tamura, Y. Takei, and Y. Okuda, 2006: Microscale analysis of severe winds within the urban canopy during a period of explosive cyclogenesis by coupling large-eddy simulation and mesoscale meteorological models. *J. Wind Eng., Japan Assoc. Wind Eng.*, **31-3**, 165−168.

Takemi, T., R. Ito, and O. Arakawa, 2016a: Effects of global warming on the impacts of Typhoon Mireille (1991) in the Kyushu and Tohoku regions. *Hydrol. Res. Lett.*, **10**, 81−87, doi:10.3178/hrl.10.81.

Takemi, T., R. Ito, and O. Arakawa, 2016b: Robustness and uncertainty of projected changes in the impacts of Typhoon Vera (1959) under global warming. *Hydrol. Res. Lett.*, **10**, 88−94, doi:10.3178/hrl.10.88.

Takemi, T., Y. Okada, R. Ito, H. Ishikawa, and E. Nakakita, 2016c: Assessing the impacts of global warming on meteorological hazards and risks in Japan: Philosophy and achievements of the SOUSEI program. *Hydrol. Res. Lett.*, **10**, 119−125, doi: 10.3178/hrl.10.119.

Yoshida, T., and T. Takemi, 2018: Properties of mixing length and dispersive stress in airflows over urban-like roughness obstacles with variable height. *SOLA*, **14**, 174−178, doi: 10.2151/sola.2018-031.

Yoshida, T., T. Takemi, and M. Horiguchi, 2018: Large-eddy-simulation study of the effects of building height variability on turbulent flows over an actual urban area. *Bound.-Layer Meteor.*, **168**, 127−153, doi:10.1007/s10546-018-0344-8.

Manuscript received 22 November 2018, accepted 28 December 2018
SOLA: https://www.jstage.jst.go.jp/browse/sola/